Effects of selected functional groups on nanoplastics transport in saturated media under diethylhexyl phthalate co-contamination conditions

Chemosphere

Yasir, Arafat Md; Ma, Jie; Ouyang, Xiaoxue; Zhao, Junying; Zhao, Yujie et al

https://doi.org/10.1016/j.chemosphere.2021.131965

Chemosphere 286 (2022) 131965

Contents lists available at ScienceDirect

Chemosphere

journal homepage: www.elsevier.com/locate/chemosphere

Effects of selected functional groups on nanoplastics transport in saturated media under diethylhexyl phthalate co-contamination conditions

Arafat Md Yasir [a,b,1], Jie Ma [a,b,*,1], Xiaoxue Ouyang [a,b], Junying Zhao [c], Yujie Zhao [a,b], Liping Weng [a,b,d,**], Md Shafiqul Islam [a,b], Yali Chen [a,b], Yongtao Li [e,f]

[a] Key Laboratory for Environmental Factors Control of Agro-Product Quality Safety, Ministry of Agriculture and Rural Affairs, Tianjin, 300191, China
[b] Agro-Environmental Protection Institute, Ministry of Agriculture and Rural Affairs, Tianjin, 300191, China
[c] School of Environmental Science and Safety Engineering, Tianjin University of Technology, Tianjin, 300384, China
[d] Department of Soil Quality, Wageningen University, Wageningen, the Netherlands
[e] College of Resource and Environmental Engineering, Jiangxi University of Science and Technology, Ganzhou, Jiangxi, 341000, China
[f] College of Natural Resources and Environment, South China Agricultural University, Guangzhou, 510642, China

HIGHLIGHTS

- PSNPs−NH_2 transport was hindered in GT and GT-DEHP-coated columns.
- GT and GT-DEHP decelerated the transport of PSNPs−COOH more than that of PSNPs.
- Deposition of PSNPs−NH_2 was largely due to its sensitivity to chemical heterogeneity.
- Quantum chemical computation was applied to study NPs transport for the first time.
- Ligand exchange caused greater deposition of PSNPs−COOH than that of PSNPs.

GRAPHICAL ABSTRACT

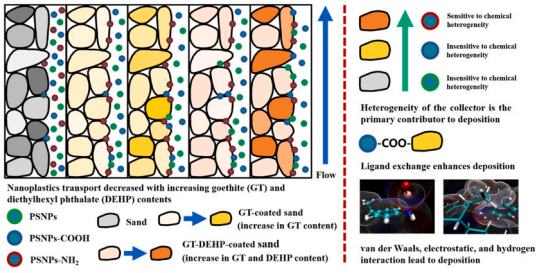

ARTICLE INFO

Handling Editor: Michael Bank

Keywords:
Nanoplastic
Functional group
Goethite
DEHP
Transport

ABSTRACT

The production and degradation of plastic remains can result in nanoplastics (NPs) formation. However, insufficient information regarding the environmental behaviors of NPs impedes comprehensive assessment of their significant threats. In this study, the transport behavior of unmodified NPs (PSNPs), carboxyl-modified NPs (PSNPs−COOH), and amino-modified NPs (PSNPs−NH_2) was investigated using column experiments in the presence and absence of goethite (GT) and diethylhexyl phthalate (DEHP). Quantum chemical computation was performed to reveal the transport mechanisms. The results showed that GT decreased the transport of NPs and the presence of DEHP decreased it further. Van der Waals forces and small electrostatic interactions coexisted between the PSNPs and GT and caused deposition. Ligand exchange caused greater deposition of PSNPs−COOH on GT-coated sand than that of PSNPs. Although hydrogen bonding existed between the DEHP and NPs with functional groups, an increase in the positive charge and chemical heterogeneity of the collector was the main

* Corresponding author. Key Laboratory for Environmental Factors Control of Agro-Product Quality Safety, Ministry of Agriculture and Rural Affairs, Tianjin, 300191, China.
** Corresponding author. Key Laboratory for Environmental Factors Control of Agro-Product Quality Safety, Ministry of Agriculture and Rural Affairs, Tianjin, 300191, China.
E-mail addresses: majie@caas.cn (J. Ma), wengliping@caas.cn (L. Weng).
[1] Arafat Md Yasir and Jie Ma contributed equally to this study and should be regarded as first joint authors.

https://doi.org/10.1016/j.chemosphere.2021.131965
Received 3 July 2021; Received in revised form 7 August 2021; Accepted 19 August 2021
Available online 19 August 2021

reason for DEHP promoting the deposition of NPs. Because of low absolute negative zeta potential values, PSNPs−NH_2 was sensitive to chemical heterogeneity, and thus fully deposited (over 96.9%) in GT and GT-DEHP-coated columns. Generally, the deposition of NPs due to chemical heterogeneity was more significant than that due to the formation of chemical bonds and van der Waals, electrostatic, and hydrogen interactions. Our results highlight that the surface charge and functional groups significantly influence the transport behaviors of NPs and elucidate the fate of NPs in the terrestrial environment.

1. Introduction

Among the various plastic contaminants, microplastics (MPs) have been investigated extensively (Wright et al., 2013; Davranche et al., 2019). Germany, Australia, Mexico, Slovenia, and Switzerland have confirmed the severity of MPs in soils, with concentrations of up to 6.7% (Hohenblum et al., 2015; Huerta Lwanga et al., 2016, 2017a; Bläsing and Amelung, 2018; Scheurer and Bigalke, 2018). However, the existence of nanoplastics (NPs) has recently been found (Gigault et al., 2018). The breakdown of larger plastic debris and aged MPs causes NPs to enter soil/agro-ecosystems (Rillig, 2012; Duis and Coors, 2016). The application of sewage sludge or biosolids from municipal wastewater treatment plants to farmlands could represent a major source of MPs in agricultural soils (Hurley and Nizzetto, 2018), with other notable inputs including plastic mulch films, greenhouse materials, soil conditioners (Duis and Coors, 2016; Horton et al., 2017), landfill leachate (Alimi et al., 2018), and irrigation activities (Bläsing and Amelung, 2018). Nanoplastics form after MPs are weathered through various mechanisms (environmental conditions), such as photochemical and physical degradation (Davranche et al., 2019), mechanical abrasion, and biological digestion (Lambert and Wagner, 2016; Dawson et al., 2018). Natural aging processes, although slow, transform plastic debris into scattered micro-to-nano-scale fragments; thus, farmlands are a major environmental reservoir of NPs (Song et al., 2019). As emerging pollutants, NPs have led to growing concern and pose potential threats to soil biota (Wu et al., 2020). For example, plastic particles significantly affect the growth rate of the earthworm *Lumbricus terrestris* (Huerta Lwanga et al., 2016), and can even enter the terrestrial food chain (Huerta Lwanga et al., 2017b) resulting in possible health risks to humans (Sharma and Chatterjee, 2017). The number of studies on the environmental behavior, fate, and toxicity of NPs has increased exponentially as they have become a significant environmental concern.

Phthalic acid esters (PAEs) are essential plasticizers used during plastic manufacturing (10–60% by weight (Zeng et al., 2009)) to increase the flexibility of polymers during processing, as well as that of the final product (Rahman and Brazel, 2004). A previous study reported that MPs and PAEs found in facility agricultural soil had a common source (Li et al., 2021). Therefore, PAEs and NPs might coexist in the environment after the weathering of plastic products. DEHP is currently one of the most frequently detected pollutants in the environment, particularly in soils (Zhou et al., 2020). In Korea and Denmark, DEHP concentrations in soil were up to 1.90 and 3.02 mg kg^{-1} respectively (NIER, 2006; Zorníková et al., 2014). The maximum concentration of DEHP in urban soil in Guangzhou was reported as 264 mg kg^{-1} (Zeng et al., 2009). Owing to its hydrophobic characteristics, DEHP tends to strongly adsorb onto soil particles (Steinmetz et al., 2016). The long-term presence of DEHP in soil may significantly affect the fate of NPs. Numerous studies have reported that the mobility of NPs varies depending on their properties (e.g. particle size and functional groups) (Dong et al., 2018, 2019; Li et al., 2019, 2020a; Song et al., 2019), the environmental conditions of water-bearing media (e.g., solution chemistry, presence of Fe_3O_4--biochar or biofilms, and the freeze-thaw environment) (Dong et al., 2018, 2019; He et al., 2020; Li et al., 2020a; Tong et al., 2020a; Alimi et al., 2021), and the cotransport of materials (e.g., CeO_2 nanoparticles, TiO_2 nanoparticles, iron oxides, biochar, bacteria, and naphthalene) (He et al., 2018; Cai et al., 2019; Li et al., 2019, 2020a; Hu et al., 2020; Tong et al., 2020b). However, the influence of DEHP on NPs transport has not yet been considered.

The functional groups of NPs might play a vital role in their transport. Most plastics in the terrestrial environment are secondary, and aging leads to the formation of plastic fragments with different functional groups (Song et al., 2019). Similar to the properties of nanoparticles, the surface functional groups of NPs might control their reactivity, stability, and mobility (Hüffer et al., 2017; Shaniv et al., 2021). Nanoplastics usually consist of a plastic core and variable functional groups that determine their effective surface charge (Nowack and Bucheli, 2007). Almost all recent studies on the aggregation and deposition of MPs/NPs have focused on spherical polystyrene (PS) particles modified with sulfate, amine, or carboxyl groups (Alimi et al., 2018). For example, carboxyl-modified NPs rapidly form 1700 nm aggregates, whereas amino-modified NPs aggregates remain stable at a smaller size of approximately 90 nm (Della Torre et al., 2014). Amino groups facilitate the adsorption of dissolved organic matter (OM) on the particle and inhibit the adsorption of Ca^{2+} and suspended OM, whereas the carboxyl group facilitates the adsorption of both (Song et al., 2019). A relatively low humic acid concentration promotes the heteroaggregation of NH_2-modified NPs to a greater extent than NPs with other functional groups, owing to the decreased electrostatic hindrance (Li et al., 2020a). Similarly, the homoaggregation of NH_2-modified NPs has been observed under a salinity of 35 PSU, and results in a decrease in its transport (Dong et al., 2019). These results suggest that the surface chemical properties of NPs affect their stability and mobility.

Soil minerals, particularly iron minerals, represent the fundamental soil properties, determining the transport of polystyrene NPs (PSNPs) due to their coupled effects on surface charges that affect the electrostatic interactions between soils and PSNPs (Wu et al., 2020). Owing to its high stability, goethite (GT) is the most widespread, highly reactive iron oxide in natural environments. GT and its colloids can strongly affect the environmental behavior of contaminants (Chen et al., 2019). In a previous study, the presence of GT did not influence the transport of 20 nm NPs; however, it could hinder the transport of large NPs (Li et al., 2019). The presence of iron minerals must be considered when investigating the migration of NPs in aqueous media.

The number of studies examining the transport, aggregation, retention, and transformation of various NPs in environmental systems is growing rapidly, and some information regarding the transport of NPs with different surface functional groups in saturated media has been reported. However, our knowledge of NPs-GT-DEHP interactions is limited. In this study, we hypothesized that the effects of GT and DEHP on the functionalization of NPs will vary. The transport of three types of NPs with different functional groups, including PSNPs, carboxyl-modified NPs (PSNPs−COOH), and amino-modified NPs (PSNPs−NH_2), was investigated in controlled laboratory column experiments using breakthrough curves (BTCs) and nanoparticle transport models, and the transport mechanism was interpreted using the DLVO theory and quantum chemical computations. Our findings provide insight into the aggregation behavior of different surface functional groups and unmodified NPs in a saturated medium, along with their interactions with DEHP, and aid in understanding the distribution and accumulation of NPs in soil environments.

2. Materials and methods

2.1. Material preparation

The transport behavior was investigated using three types of 50 nm PSNP spheres including PSNPs, PSNPs−COOH, and PSNPs−NH_2 (Huge Biotechnology Co., Ltd). Approximately 100 mmol g^{-1} carboxyl and amino groups were introduced to the NP surfaces through reactions with acrylic acid and ethylenediamine, respectively. The functional group information of NPs produced by this company is provided in a previous article (Li et al., 2020a). The concentration of the stock solutions was 2.5% w/v, and they were diluted to obtain a target concentration of 200 mg L^{-1}. The concentrations of the NPs suspensions were determined by measuring the extinction at 300 nm using a spectrophotometer (UV-2700, Shimadzu), based on the linear calibration curves between the absorbencies and standards (Shani et al., 2008). The linear calibration curves for the NPs concentrations are shown in Fig. S1. The settling curve showed that the three kinds of NPs were very stable in water at pH 7.5 (Fig. S2). Goethite was synthesized by the procedure described in Schwertmann and Cornell (2008). Briefly, GT was precipitated by titrating dissolved Fe $(NO_3)_3{\cdot}9H_2O$ with NaOH to a pH 12. The suspension was then aged for 4 d and dialyzed until EC < 10 μS cm^{-1}. Then the GT was then freeze-dried and ground to a fine powder for further use. The particle size of GT in water at pH 7.5 was ~304.2 ± 5.8 nm, similar to that in our previous study (Ma et al., 2020). Analytically pure DEHP was used to simulate the impact of phthalates on NPs transport.

2.2. Transport experiment

Column experiments were conducted in glass chromatographic columns with a length and inner diameter of 10 and 1.5 cm, respectively. Quartz sand with an average size of 337.5 μm was packed in the column as the standard porous media, which was first immersed in 6-M HCl for at least 24 h for cleaning, and then repeatedly rinsed with Milli-Q water. Goethite -coated sand or GT-DEHP-coated sand were prepared by mixing. Different amounts of sand, GT, and DEHP were mixed with 10% Milli-Q water to make the material adhere to the surface of the sand. The filler mixture ratios (mass ratio) are presented in Table 1. Then quartz sand or mixed sand was wet-packed into each glass column. The effective porosity and bulk density of the packed columns were 0.45 ± 0.02 cm^3 cm^{-3} and 1.43 ± 0.05 g cm^{-3}, respectively. After packing, the columns were pre-conditioned with 15 pore volumes (PVs) of Milli-Q water with an IS of 0.1 mM NaCl using a peristaltic pump (BT-100 1F, Longer) in the up-flow mode. Following pre-equilibration, 10 PVs of NPs with an IS of 0.1 mM NaCl were injected into the columns, followed by elution with 5 PVs of Milli-Q water with the corresponding pH and IS at a constant Darcy velocity of 0.568 cm min^{-1}. All column experiments were conducted at a pH of 7.5. The NPs concentrations in the effluent were measured for each PV using a spectrophotometer. The zeta potentials of the NPs and coated sand (after milled) were measured in triplicate using a dynamic light-scattering analyzer (Zetasizer Nano ZS, Malvern) (Table 1). The zeta potentials of the NPs were similar to those determined in a previous study at pH 7.5 (Li et al., 2020a). Then, the measured mean zeta potentials were used to calculate the DLVO interaction energy. Following the completion of the transport experiments, the deposition of NPs in the 0–2.5 cm columns was observed using scanning electron microscopy (SEM) with a Zeiss Merlin Compact (at 15 kV) and energy dispersive spectroscopy (EDS) (OxfordX-MAX, Zeiss).

Table 1
Zeta potential of NPs, sand, and coated sand at pH 7.5

NPs and sand	Zeta potential
PSNPs	−44.1 ± 1.7
PSNPs-COOH	−47.8 ± 1.0
PSNPs-NH_2	−27.7 ± 0.2
Quartz sand	−45.6 ± 2.3
Quartz sand-0.2% GT	13.1 ± 1.4
Quartz sand-0.5% GT	18.0 ± 0.5
Quartz sand-2% GT	20.6 ± 1.4
Quartz sand-0.2% GT-0.05% DEHP	27.3 ± 0.9
Quartz sand-0.5% GT-0.05% DEHP	28.8 ± 0.5
Quartz sand-0.5% GT-0.2% DEHP	30.5 ± 0.4

2.3. Model and data analysis

2.3.1. Transport model

Before the NPs transport experiment, a conservative tracer checked the longitudinal dispersity of the columns (Qian et al., 2020). A conservative tracer can check the hydraulic characteristics, including the longitudinal dispersity, of the columns before the nanoparticle transport experiments. The transport data were simulated by the nanoparticle transport model, which included two-site kinetic retention to describe nanoparticle transport and retention in the column experiments (Bradford et al., 2003). For the first kinetic Site-1, the time-dependent retention is taken into account, assuming reversible retention using first order retention (k_{1a}) and detachment (k_{1d}) coefficients. For the second kinetic Site-2, depth-dependent retention is considered, assuming irreversible retention using a first-order retention coefficient (k_{2a}). Detailed equations and relative parameters are exhibited in Supplementary Material S3.

2.3.2. DLVO theory

The Derjaguin-Landau-Verwey-Overbeek (DLVO) theory performs a function in calculating the total nanoparticle-sand interaction energy by adding Lifshitz-van der Waals (LW) to electrical double layer (EDL) interactions. The total calculations of LW and EDL interactions as a sphere-plate geometry system (Derjaguin and Landau, 1941; Verwey and Overbeek, 1948) were utilized to predict the interactions between NPs and quartz sand. Details of the DLVO theory and operative equations are presented in Supplementary material S4.

2.3.3. Quantum chemical computation

Quantum chemical calculations were used to explain the interaction of NPs with GT or DEHP, which play a key role in NPs transport. The configurations of the molecules were determined using the Molclus program (http://www.keinsci.com/research/molclus.html), molecular formulas of NPs monomer, GT, and DEHP are presented in Fig. S3. After generating the original configurations, they were each optimized based on the all-electron density functional theory (DFT) at the B3LYP/6-311G (d) level using the quantum chemistry Gaussian 16 software package (Frisch et al., 2016). The optimized configuration with the lowest energy was then further optimized at the B3LYP/6-311G(d) level. Grimme's D3BJ dispersion was used to describe intermolecular interactions, and the binding energies were calculated using the following equation (1):

$$\text{Binding energy} = E_{complex} - (E_{fragment1} + E_{fragment2}) \quad (1)$$

where $E_{complex}$ is the energy of a complex composed of two molecules, and $E_{fragment1}$ and $E_{fragment2}$ are the energies of a single molecule corresponding to different systems.

To observe the nature of the interaction more clearly, the electrostatic potential (ESP) was analyzed using Multiwfn software (Lu and Chen, 2012). The complex structures and contour surface of ESP were visualized using Visual Molecular Dynamics (VMD) software (Humphrey et al., 1996).

Mayer bond orders (Mayer, 1983, 1984) were calculated based on the following equation (2) (Poater et al., 2012):

$$M_{AB} = 2\sum_{\mu\in A}\sum_{\vartheta\in B}\left[(P^{\alpha}S)_{\mu\vartheta}(P^{\alpha}S)_{\vartheta\mu} + (P^{\beta}S)_{\mu\vartheta}(P^{\beta}S)_{\vartheta\mu}\right] \quad (2)$$

where S is the atomic orbital overlap matrix and P^{α} and P^{β} are the density matrices for the α and β electrons, respectively.

3. Results and discussion

3.1. Effect of GT on nanoplastics transport

The influence of different functional group-associated NPs on their transport and deposition in porous media was examined in the presence or absence of different concentrations of GT. The observed and simulated BTCs of NPs transport are shown in Fig. 1, and the fitted parameters of the columns are presented in Table 2. Variations in the GT content and surface functionality of NPs influenced their transport in the columns, as indicated by the changes in the recovery rates of the NPs in the effluent, which ranged from 1.6% to 98.7% in different columns. The rapid transport of NPs or MPs in quartz sand columns has been widely reported (Shen et al., 2011; Dong et al., 2018; Li et al., 2019; Song et al., 2019; Hu et al., 2020; Tong et al., 2020b). A negative charge and relatively smooth surface of sand make it difficult to retard their transport. The DLVO theory explains the transport of NPs in the columns, and the primary energy barriers (28.5–45.6 kT) were not conducive to NPs deposition on the sand (Fig. S4). The NPs and quartz sand were negatively charged (Table 1), and the repulsive electrostatic forces between the negatively charged NPs and porous sand media caused high k_{1d}/k_{1a} values (1.26–3.44) (Table 2) enhancing the transport of NPs (Ma et al., 2016, 2018; Peng et al., 2017). All three NPs broke through the media, with only approximately 1.3–7.5% of the NPs deposited in the columns (Fig. 2 and Table 2).

In all combinations, GT-coated sand (0.2%, 0.5%, and 2%) exhibited a positive zeta potential (13.1–20.6 mV) (Table 1), causing attraction between the collector and negatively charged NPs. In particular, the increase in GT content from 0 to 0.5% changed the electrical properties of the sand from negative to positive, thus causing the marked retardation of NPs transport. The BTCs of PSNPs and PSNPs–COOH in the presence of GT gradually decreased with increasing additive concentration. The addition of 0.2% GT in the column analogously immobilized PSNPs and PSNPs–COOH by approximately 31.8% and 34.0%, respectively. Under the addition of 0.5% GT, the small actual increment of GT and their mutual stacking, did not have many additional deposition points. Therefore, a breakthrough plateau developed that was smaller than that under 0.2% GT, and trapped approximately 8.3% and 11.7% more PSNPs and PSNPs–COOH in the column, respectively. The maximum deposition of PSNPs (57.5%) and PSNPs–COOH (67.0%) occurred in the 2% GT-coated sand column. Moreover, the BTCs of PSNPs and PSNPs–COOH decreased as the k_{1a} values increased (Fig. 1a and b, and Table 2), indicating that GT had a greater influence on the deposition of PSNPs and PSNPs–COOH on the reversible site with increasing GT content. However, the low k_{1d} values (0.000–0.003 min^{-1}) suggested little release of PSNPs and PSNPs–COOH. The gradually increasing k_{2a} values indicated that irreversible PSNPs–COOH deposition also increased with increasing GT content. Similarly, the iron oxide-coated quartz sand column blocked most of the transport of TiO_2 nanoparticles (83–95%) (Han et al., 2014). A previous study reported that positively charged GT could decrease the transport of MPs by changing their sizes, causing heteroaggregation, and enhancing their adsorption onto sand (Li et al., 2019). Another previous study reported that Fe mineral colloids and NPs can cause hetero-aggregation (Oriekhova and Stoll, 2018). However, the influence of GT on NPs was minimal. A larger amount of GT was applied in this study, and its influence on the NPs was gradually revealed. The surfaces of heterogeneously charged granular media present in the natural environment typically carry iron oxide patches (Song et al., 1994; Han et al., 2014) and often acquire a net positive charge in environmental solutions (Wang et al., 2012; Han et al., 2014) due to their high pH_{PZC}. Such minerals have been found to enhance the retention of negatively charged colloids and nanoparticles (Foppen et al., 2006; Wang et al., 2012). In this study, the transport of PSNPs and PSNPs–COOH was not completely hindered as GT did not fundamentally change the stability and aggregation of small-sized NPs with a highly negative zeta potential (Li et al., 2019).

The incorporation of GT at all tested concentrations (0.2–2%) completely blocked the transport of PSNPs–NH_2, and only small amounts were recovered (1.6–2.8%) from the effluent following negligible breakthrough (Fig. 1c). The transport ability of the three kinds of NPs was similar to those transport in natural porous media (Shaniv et al., 2021). Moreover, a previous study reported that the effect of ions (Na^+, K^+, and Mg^{2+}) and Suwannee River humic acid decreased the stability and mobility of NH_2-modified NPs (Dong et al., 2019), showing that the stability of NH_2-modified NPs is easily affected by environmental conditions. PSNPs–NH_2 had a comparatively lower negative zeta potential (−27.7 mV) than PSNPs (−44.1 mV) and PSNPs–COOH (−47.8 mV). At the pH value of the solution in the study, low-negatively-charged PSNPs–NH_2 were readily electrically neutralized by GT. Similarly, a neutral environment facilitated the heteroaggregation of PSNPs–NH_2 and CeO_2 NPs (Li et al., 2020a). Previous studies demonstrated that surface charge heterogeneity can locally decrease the repulsive energy barrier, thereby increasing colloid attachment under unfavorable chemical conditions (Zhang et al., 2019; Li et al., 2020b). A previous study also found that when MPs coexisted with TiO_2 nanoparticles, the formation of larger nTiO_2-MPs heteroaggregate clusters led to fewer repulsive interactions with quartz sand; thus, they could be easily retained (Cai et al., 2019). In this study, under hydraulic flushing, a small number of GT nanoparticles might drop from the sand surface (Chen et al., 2019), and this part of GT also contributed to the NPs deposition.

The surface roughness might also play a crucial role in NPs transport in GT-coated sand. Previous studies have reported that a high collector surface roughness decreases the repulsive interactions between the collector and colloid, such that greater colloid attachment was expected in collectors with a higher roughness, and changes in the transport behavior of colloids under different solution conditions decreased in rougher porous media (Shellenberger and Logan, 2002; Shen et al., 2011). The DLVO results showed that the primary energy barrier between the GT-coated sand and NPs disappeared (Fig. S4), indicating the absence of repulsion. Generally, nanoparticles are not easily transported quickly in the absence of a primary barrier (Ma et al., 2016). However, PSNPs and PSNPs–COOH maintained relatively rapid transport in this

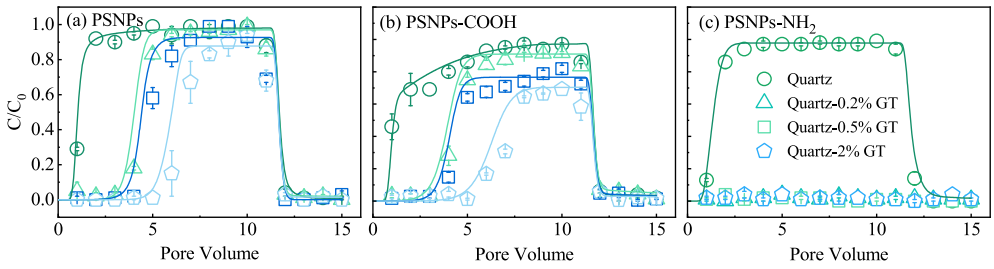

Fig. 1. Breakthrough curves of PSNPs, PSNPs–COOH, and PSNPs–NH_2 transport in pure sand and GT-coated columns at a pH of 7.5. The symbols and solid lines indicate the observed and simulated data, respectively, and the error bars represent the range of replicate experiments ($n \geq 2$).

Table 2
Fitted parameters of transport of PSNPs, PSNPs–COOH, and PSNPs–NH_2 in different ratio GT-coated sand columns at pH 7.5.

NPs	Column	k_{1a} [a] (min^{-1})	k_{1d} [b] (min^{-1})	k_{2a} [c] (min^{-1})	R^2 [d]	Recovery [e] (%)
PSNPs	Quartz sand	0.033 ± 0.017	0.168 ± 0.162	0.024 ± 0.024	0.995 ± 0.003	98.7 ± 0.1
	Quartz sand-0.2% GT	1.502 ± 0.024	0.001 ± 0.000	0.045 ± 0.014	0.997 ± 0.003	68.2 ± 1.6
	Quartz sand-0.5% GT	1.909 ± 0.738	0.000 ± 0.000	0.115 ± 0.023	0.990 ± 0.003	59.9 ± 2.3
	Quartz sand-2% GT	3.127 ± 0.909	0.000 ± 0.000	0.196 ± 0.022	0.991 ± 0.003	42.5 ± 2.0
PSNPs-COOH	Quartz sand	0.074 ± 0.001	0.094 ± 0.001	0.000 ± 0.000	0.975 ± 0.014	92.5 ± 1.5
	Quartz sand-0.2% GT	1.026 ± 0.197	0.003 ± 0.001	0.142 ± 0.014	0.995 ± 0.003	66.0 ± 0.0
	Quartz sand-0.5% GT	1.408 ± 0.051	0.002 ± 0.002	0.402 ± 0.112	0.985 ± 0.002	54.3 ± 0.6
	Quartz sand-2% GT	1.400 ± 0.123	0.002 ± 0.002	0.525 ± 0.064	0.984 ± 0.000	33.0 ± 0.5
PSNPs-NH_2	Quartz sand	0.255 ± 0.062	0.454 ± 0.425	0.033 ± 0.001	0.996 ± 0.002	98.4 ± 1.2
	Quartz sand-0.2% GT					2.5 ± 0.3
	Quartz sand-0.5% GT					1.6 ± 0.3
	Quartz sand-2% GT					2.8 ± 0.1

[a] The first-order retention coefficient on Site-1.
[b] The first-order detachment coefficient on Site-1.
[c] The first-order retention coefficient on Site-2.
[d] Squared Pearson's correlation coefficient.
[e] Recovery of NPs in the effluent.

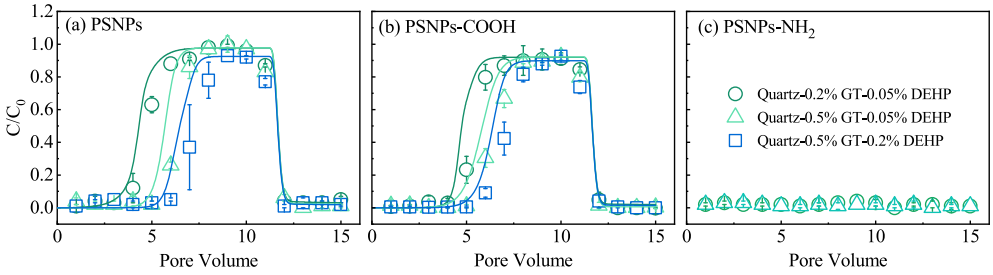

Fig. 2. Breakthrough curves of PSNPs, PSNPs–COOH, and PSNPs–NH_2 transport in GT-DEHP-coated columns at a pH of 7.5. The symbols and solid lines indicate the observed and simulated data, respectively, and the error bars represent the range of replicate experiments ($n \geq 2$).

study, suggesting that the DLVO theory does not adequately explain the experimental phenomenon. Non-DLVO interactions, such as chemical bonding, hydrogen forces, and π-π interactions, also participate in the attachment and transport of nanoparticles (Kamrani et al., 2018; Tan et al., 2019; Abdoul Magid et al., 2021), which will be discussed later.

3.2. Effect of DEHP on nanoplastics transport

The influence of DEHP on the transport of NPs with different functional groups in the GT-coated sand column was examined. The observed and simulated transport BTCs of the NPs are shown in Fig. 2, and the fitted parameters of the columns are presented in Table 3. The BTCs obtained in the presence of DEHP under most conditions were similar to those without DEHP (Figs. 1 and 2). The breakthrough plateaus of the PSNPs and PSNPs–COOH in Fig. 2a and b retreated gradually as the GT and DEHP contents increased. The decreasing recoveries and increasing k_{1a} values in the presence of DEHP (Table 3) indicated that it enhanced the deposition of PSNPs and PSNPs–COOH on the reversible site. The higher BTC plateaus and lower k_{2a} values than those in the absence of DEHP (Figs. 1b and 2b, and Tables 2 and 3) suggested that the deposition of PSNPs–COOH on the irreversible sites decreased. Similar to GT-coated columns, the low k_{1d} values (0.000–0.001 min^{-1}) also suggested little release of PSNPs and PSNPs–COOH. As DEHP is highly intermiscible with plastic molecules, the retention of NPs is substantial, even at a low DEHP content (0.05%). The addition of DEHP trapped 2.4–19.2% and 9.1–14.8% more PSNPs and PSNPs–COOH than that in the absence of DEHP under the same GT content, respectively (Tables 2 and 3), suggesting that the hindering effect of DEHP on the transport of PSNPs and PSNPs–COOH was enhanced as the DEHP concentration increased. Moreover, the effect of a high DEHP content (0.2%) on the transport of PSNPs–COOH (14.8%) was smaller than that on the transport of PSNPs (19.2%). The differences between PSNPs and PSNPs–COOH indicated that the transportation of different NPs depended on their surface functionalities (Fig. 2). No BTCs were produced for PSNPs–NH_2 (Fig. 2c) and more than 95% of the NPs were retained (Table 3). It was difficult to identify the role of DEHP in PSNPs–NH_2

Table 3
Fitted parameters of transport of PSNPs, PSNPs–COOH, and PSNPs–NH_2 in different ratio GT-DEHP-coated sand columns at pH 7.5

NPs	Column	k_{1a} (min^{-1})	k_{1d} (min^{-1})	k_{2a} (min^{-1})	R^2	Recovery (%)
PSNPs	Quartz sand-0.2% GT-0.05% DEHP	1.695 ± 0.976	0.001 ± 0.000	0.035 ± 0.032	0.995 ± 0.001	65.8 ± 0.6
	Quartz sand-0.5% GT-0.05% DEHP	2.198 ± 0.406	0.001 ± 0.000	0.034 ± 0.034	0.997 ± 0.002	51.0 ± 3.1
	Quartz sand-0.5% GT-0.2% DEHP	2.988 ± 0.020	0.001 ± 0.000	0.116 ± 0.005	0.998 ± 0.001	40.7 ± 4.5
PSNPs-COOH	Quartz sand-0.2% GT-0.05% DEHP	2.901 ± 1.282	0.001 ± 0.001	0.127 ± 0.091	0.993 ± 0.002	55.8 ± 2.1
	Quartz sand-0.5% GT-0.05% DEHP	1.407 ± 0.025	0.000 ± 0.000	0.122 ± 0.013	0.996 ± 0.002	45.2 ± 1.1
	Quartz sand-0.5% GT-0.2% DEHP	2.081 ± 0.489	0.000 ± 0.000	0.159 ± 0.032	0.997 ± 0.003	39.5 ± 0.9
PSNPs-NH_2	Quartz sand-0.2% GT-0.05% DEHP					3.1 ± 0.6
	Quartz sand-0.5% GT-0.05% DEHP					2.6 ± 0.9

transport as it can be completely hindered by GT.

Iron minerals can adsorb plasticizers, including DEHP (Witthayaphirom et al., 2020). The zeta potentials of all GT-coated sand media increased in the presence of DEHP (Table 1), indicating that they were positively charged and that cation bridging might have occurred between the GT and DEHP (Foppen et al., 2006). Increasing the DEHP content in conjunction with GT slightly increased the positive zeta potentials (Table 1) and roughness of the sand. Moreover, the presence of DEHP increased the heterogeneity of the porous media. Thus, the interaction between NPs and the collector was significantly attractive, particularly at high GT and DEHP contents.

3.3. Nanoplastics deposition

The depositional morphology of the NPs was observed using SEM (Fig. 3). In accordance with the transport characteristics, the NPs were readily deposited adjacent to the column inlet (0–2.5 cm). The SEM image is not shown because only a few NPs were deposited onto the pure sand. The small spheres highlighted on the rough surfaces in the SEM images indicated that more NPs were deposited on the GT-DEHP-coated sand (Fig. 3). Furthermore, the SEM results showed that smaller NPs were adsorbed on the surface of the larger GT. In PSNPs–0.5% GT sand, PSNPs aggregates were bound to GT clusters in a sparse aggregation state (Fig. 3a). In the PSNPs−COOH–0.2% GT-coated sand, PSNPs−COOH-GT aggregates were very clear due to the relatively low GT content, and each PSNPs−COOH sphere was deposited on GT (Fig. 3b). Similarly, the PSNPs–NH_2 clusters were attached to GT under a content of 0.5% (Fig. 3c), forming larger and more compact hetero-aggregates. A previous study also reported that adsorption occurs between Fe oxides and NPs (Li et al., 2019), as well as between Fe and OM (Chen et al., 2014). In the presence of DEHP, the initially clear outline of the GT became blurred, indicating that DEHP adsorbed to the GT (Fig. S5). Following the transport experiments, NPs were deposited on the GT-DEHP-coated sand more easily than on the GT-coated sand (Fig. 3d, e, and f). The deposited NPs exhibited vague outlines due to the DEHP, and the degree of fuzziness increased with increasing DEHP concentration. Consistent with the transport results, the deposition amounts of NPs gradually increased in the following order: PSNPs < PSNPs–COOH < PSNPs–NH_2.

According to previous studies, the surface charges of commonly used collectors exhibit microscopic heterogeneities, which might have a profound influence on colloid adhesion (Li et al., 2004; Tufenkji and Elimelech, 2004). Moreover, some observations indicated that the collector surface roughness promoted colloid or nanoparticle deposition (Bradford et al., 2003, 2017; Shen et al., 2011). According to the SEM images, it was obvious that more GT had a coarser surface due to their mutual stacking (Fig. 3). Higher GT and DEHP contents resulted in increased chemical and physical heterogeneity. Therefore, the maximum NPs deposition was observed on the 0.5% GT and 0.2% DEHP-coated sand. DEHP introduced a more positive charge to the GT-coated collectors (Table 1), resulting in higher electrostatic attraction to the negatively charged NPs. Therefore, chemical heterogeneity might play a more important role in NPs retention. The effect of physical heterogeneity on NPs deposition could be relatively small; however, the effect of roughness should not be ignored. A previous study reported that biofilm increases the deposition of NPs and MPs in porous media owing to the narrowed flow path and increased surface roughness (He et al., 2020). The roughness of the collector can promote interactions that cause deposition, even under electrostatically unfavorable conditions (Bradford et al., 2017). Undoubtedly, higher GT and DEHP contents could increase the roughness fraction and height of porous media, enhancing NPs deposition. Because of GT or GT-DEHP partial coating, NPs might first saturate GT or GT-DEHP as deposition sites. Therefore, the interactions between NPs and GT/DEHP were the key to explaining the mechanism of transport.

3.4. Interactive mechanism between nanoplastics and goethite/DEHP

Quantum chemical computations were conducted to further investigate the mechanism underlying the interactions between NPs and GT or DEHP, as this method is widely used to calculate the interactions between NPs and other pollutants (Cortes-Arriagada, 2021; Gao et al., 2021a, 2021b). Different from the LW and EDL of DLVO theory, this method explains the effect of functional groups on NPs transport via a more microscopic perspective. In the PSNPs and GT systems, the surface electrostatic potential of the PSNPs molecule was almost white, with only a few positive and negative regions (Fig. 4a and b). The molecular surface of the GT exhibited distinct positive and negative charge distributions, and the electrostatic potential between the two molecules partially overlapped on the surface. The interaction in the system was

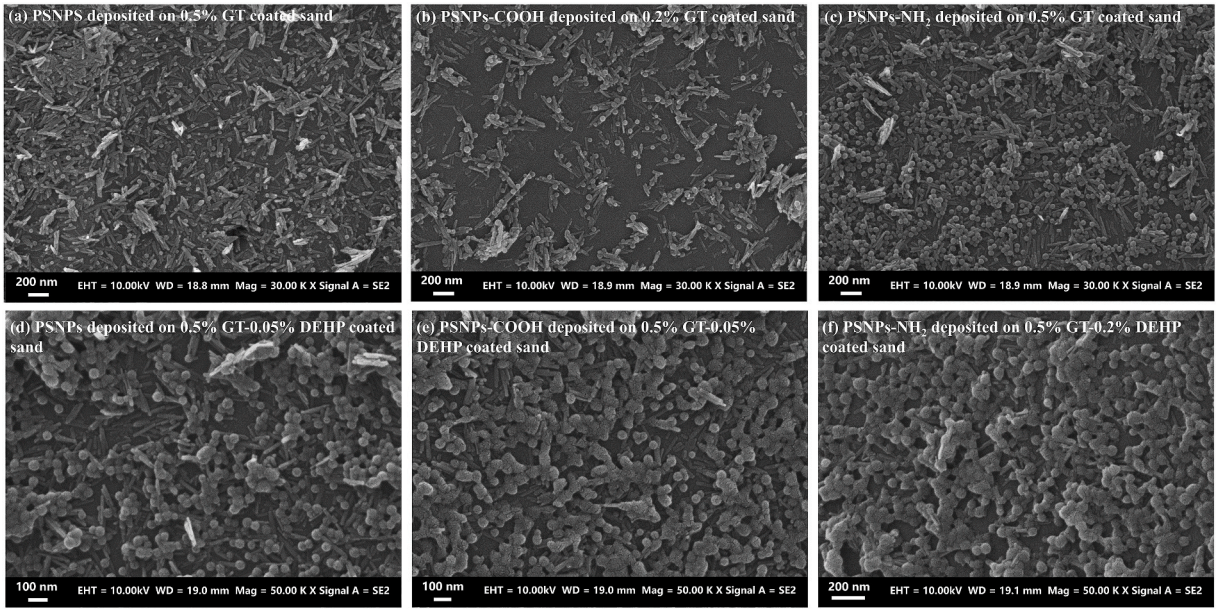

Fig. 3. SEM images of PSNPs (a and d), PSNPs–COOH (b and e), and PSNPs–NH_2 (c and f) deposited on GT-coated (a, b, and c) and GT-DEHP-coated (d, e, and f) sand.

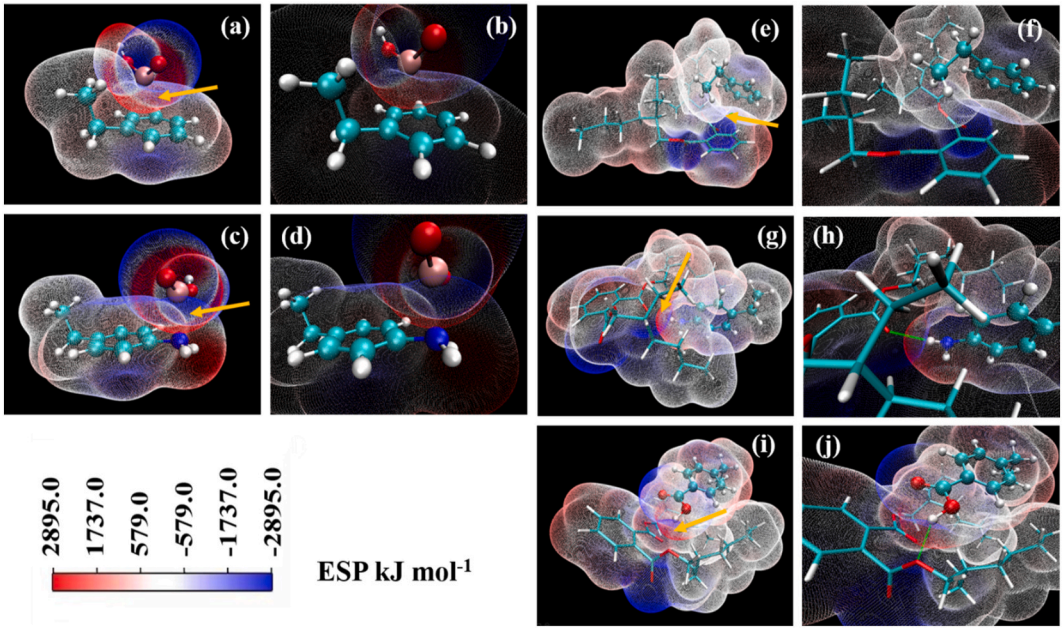

Fig. 4. Cluster model of the structures of PSNPs and GT (a and b), PSNPs−NH_2 and GT (c and d), PSNPs and DEHP (e and f), PSNPs−NH_2 and DEHP (g and h), and PSNPs−COOH and DEHP (i and j). The blue-green, red, gray, and pink spheres/sticks represent C, O, H, and Fe, respectively, whereas the emerald-green lines represent hydrogen bonds. ESP refers to the electrostatic potential of the macromolecules. (For interpretation of the references to colour in this figure legend, the reader is referred to the Web version of this article.)

concentrated in the benzene ring, indicating that van der Waals forces formed the main interactions between the two molecules, and there was a small amount of electrostatic interactions. In the PSNPs and DEHP systems, the electrostatic surface potential of the PSNPs molecules showed only a few positive and negative regions and there was almost no overlap in electrostatic potential on the surfaces of the PSNPs and DEHP (Fig. 4e and f), indicating that there were van der Waals interactions between the two molecules but few electrostatic interactions (Gao et al., 2021a). PSNPs are polarized when close to the DEHP polar group, and then, the induced dipole and inherent dipole are attracted to each other to generate an induced force, whereas PSNPs close to the hydrophobic end of DEHP might cause inconsistent instantaneous positive and negative charge centers of gravity, generating transient dipoles and a dispersion force (Gao et al., 2021a). The induced force and dispersion force constitute van der Waals interaction. The binding energy between the PSNPs and DEHP was −57.6 kJ mol^{-1} (Table S1). The absolute value was smaller than that between the PSNPs and GT, (−143.7 kJ mol^{-1}), indicating that the latter exhibited more prominent interactions.

In the PSNPs−NH_2 and GT systems, the electrostatic potential of the two molecules (red and blue regions) overlapped in opposite directions, and the interaction was concentrated in the NH_2 functional group, indicating that strong electrostatic interactions formed between the NH_2 and Fe functional groups, as well as van der Waals interactions (Fig. 4c and d). Relatively strong electrostatic interactions between the two molecules also occurred in the PSNPs−NH_2 and DEHP systems. Moreover, the NH_2 functional groups and DEHP formed clear hydrogen bonds (Fig. 4g and h). The binding energy between the PSNPs−NH_2 and DEHP was −79.4 kJ mol^{-1}, which was smaller than that between PSNPs and GT (−159.0 kJ mol^{-1}) (Table S1), indicating that more interactions occurred between the PSNPs−NH_2 and GT. Similar to PSNPs−NH_2 and DEHP, van der Waals, electrostatic, and hydrogen bonding interactions occurred between the PSNPs−COOH and DEHP with a binding energy of −93.3 kJ mol^{-1} (Table S1). The interaction between the NPs and DEHP gradually increased in the following order: PSNPs < PSNPs–NH_2 < PSNPs–COOH.

As the COOH functional group easily undergoes ligand exchange with GT, the Mayer bond levels between the atoms of the formed coordination complex were further analyzed using Multiwfn (Fig. 5). The Mayer bond order (Mayer, 1983, 1984) can be used to evaluate the molecular bond strengths in the reactions (Poater et al., 2012). During the interaction process between PSNPs−COOH and GT, the H atom on the COOH functional group was transferred to the O atom of the GT and the formation of H_2O was separated. The Fe atom in the GT molecule and PSNPs−COOH shared an O atom, forming the PSNPs–COO–(FeO) coordination complex. The Mayer bond level represents the logarithm of the shared electrons between two atoms in the complex and indicates their bonding situation. By comparing the Mayer bond levels between atoms near the dehydration coordination, it can be seen that the logarithm of the shared electrons between the H and O atoms originally on the COOH functional group decreased significantly (0.171) and was smaller than that for the newly formed OH bond (0.604) with OH separated from the GT. The O atom moved away from the Fe atom following the formation of water molecules, as confirmed by the low Mayer bond level between the Fe and O atoms (0.158), which was much smaller than the original Mayer bond of Fe–OH (0.671). An Fe–O bond appeared at the O atom shared by GT and COOH, and the two atoms shared 0.196 pairs of electrons (approximately 0.4 shared electrons), indicating the formation of a coordination bond. Similarly, GT attracts negatively charged natural organic matter with polar functional groups through ligand exchange and electrostatic interactions in the soil (Safiur

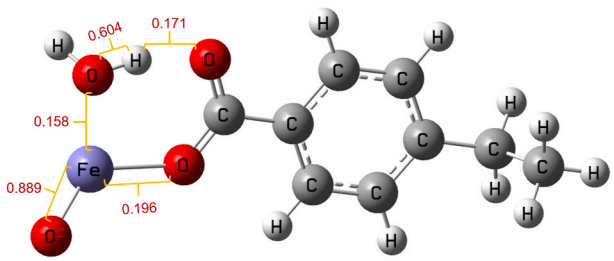

Fig. 5. Mayer bond level between the atoms of the coordination complex following the reaction of PSNPs–COOH and GT.

Rahman et al., 2013; Wang et al., 2019). The coordination bond could result in the irreversible deposition of PSNPs−COOH, and van der Waals and electrostatic interactions might result in reversible deposition. The deposition of PSNPs−COOH on two types of retention sites is consistent with the transport results.

The interactions between NPs and GT gradually increased in the following order due to the coordination bond: PSNPs < PSNPs–NH_2 < PSNPs–COOH. This explained why PSNPs–COOH are more likely to deposit on GT-coated sand than PSNPs. However, the order of interactions between PSNPs–NH_2 and GT was not consistent with its transport characteristics. In addition to the functional group differences, the largest difference between the PSNPs–NH_2 and the other two types of NPs was the low negative potential (Table 1), which increased the likelihood of PSNPs–NH_2 producing heteroaggregation under the influence of GT. It has previously been reported that divalent electrolytes result in a lower zeta potential for CeO_2 nanoparticles and further cause their heteroaggregation in the presence of alginate and iron (III) oxide in lake water (Oriekhova and Stoll, 2019). Although ions are inducers, the low zeta potential is the main cause of CeO_2 heteroaggregation. For NPs, NH_2-modified NPs with a low negative zeta potential are highly sensitive to humic acids and ionic strength, and thus have previously exhibited strong heteroaggregation and deposition potential (Dong et al., 2019; Li et al., 2020a). In this study, the retention of PSNPs–NH_2 due to chemical heterogeneity was stronger than that due to ligand exchange and electrostatic interactions. The elongated morphology of GT might enhance its chemical heterogeneity (Ma et al., 2020) and further improve the deposition of PSNPs–NH_2.

The interaction energy between NPs and DEHP increased in the following order: PSNPs < PSNPs–NH_2 < PSNPs–COOH. The hydrogen bond and electrostatic interactions formed by the functional group and DEHP resulted in the enhanced interactions. Although these interactions contributed to the deposition of PSNPs–NH_2 and PSNPs–COOH, there were fewer interactions between the NPs and DEHP than between the NPs and GT. The interaction between NPs and mixed GT and DEHP decreased, and the degree of decrease increased with increasing DEHP content; however, the retention of PSNPs and PSNPs–COOH increased. This indicates that the high positive zeta potential of GT-DEHP-coated sand and the increase in heterogeneity promoted the deposition of NPs. Similarly, Fe minerals and organic materials have also been found to contribute to the deposition of NPs. PSNP aggregation was achieved at a higher concentration of 20 mg L^{-1} when interacting with Fe_2O_3 and NOM (Oriekhova and Stoll, 2018). Moreover, Fe_3O_4-biochar could increase the adsorption capacity of porous media, contributing to the enhanced deposition of NPs (Tong et al., 2020a). Comparing the BTCs of PSNPs–COOH with and without the addition of DEHP, although the recovery of the NPs in the effluent decreased in the presence of DEHP (Tables 2 and 3), the height of the BTC increased (Figs. 1b and 2b), indicating that the deposition of PSNPs–COOH was converted to reversible retention. This was attributed to the coverage of DEHP, which reduced the ligand exchange of PSNPs–COOH with GT.

4. Conclusion

The fate of NPs affected by co-contaminants in the soil environment must be understood. This study demonstrates the transport of NPs in the presence of GT and DEHP and the effect of functional groups on the deposition of NPs on the collector surfaces. Our results showed that distinctly different transport behaviors occurred in the three types of NPs, suggesting that the different functionalities and their controlled surface properties played dominant roles in the transport of NPs that were highly sensitive to GT and DEHP. NPs are most likely to move long distances in the absence of GT, whereas the presence of GT and DEHP restricts their transport. PSNPs−NH_2 were completely immobilized (>96.9%) in the GT and GT-DEHP-coated columns. GT and GT-DEHP decelerated the transport of PSNPs−COOH to a greater extent than that of PSNPs, with a difference in recovery of 1.2–10.0%. Although this study failed to explain this phenomenon using the DLVO theory, the quantum chemical computation calculated the ability of different NPs to bind to GT and DEHP. The interaction between PSNPs and GT mainly occurred in the benzene ring, and van der Waals forces and small electrostatic interactions coexisted. Ligand exchange caused a greater deposition of PSNPs−COOH than PSNPs on GT-coated sand. Sensitivity to chemical heterogeneity was the main factor promoting the deposition of PSNPs−NH_2 in the presence of GT. Although hydrogen bonding was present, fewer interactions occurred between NPs and DEHP than between NPs and GT. However, DEHP caused chemical heterogeneity and promoted the deposition of NPs. Generally, the deposition caused by chemical heterogeneity was more significant than that caused by the formation of chemical bonds, van der Waals forces, and electrostatic and hydrogen interactions. This behavior reduced the transport risk of NPs in the soil. Therefore, the results of this study provide valuable insights into the transport and retention of NPs in natural soils.

Author statement

Arafat Md Yasir: Resources, Investigation, Formal analysis, Writing-original draft. Jie Ma: Conceptualization, Methodology, Writing-original draft, Funding acquisition. Xiaoxue Ouyang: Writing-review & editing. Junying Zhao: Writing-review & editing. Yujie Zhao: Writing-review & editing. Liping Weng: Conceptualization, Methodology, Funding acquisition. Md Shafiqul Islam: Writing-review & editing. Yali Chen: Writing - review & editing. Yongtao Li: Writing-review & editing.

Declaration of competing interest

The authors declare that they have no known competing financial interests or personal relationships that could have appeared to influence the work reported in this paper.

Acknowledgments

The study is financially supported by the Natural Science Foundation of Tianjin (19JCQNJC08500), Open Fund of Key Laboratory for Environmental Factors Control of Agro-Product Quality Safety, Ministry of Agriculture and Rural Affairs (2020-hjyzfp-70201801), and the Central Public-interest Scientific Institution Basal Research Fund (2020-jbkyywf-mj).

Appendix A. Supplementary data

Supplementary data to this article can be found online at https://doi.org/10.1016/j.chemosphere.2021.131965.

References

Abdoul Magid, A.S.I., Islam, M.S., Chen, Y., Weng, L., Li, J., Ma, J., Li, Y., 2021. Enhanced adsorption of polystyrene nanoplastics (PSNPs) onto oxidized corncob biochar with high pyrolysis temperature. Sci. Total Environ. 784.

Alimi, O.S., Farner Budarz, J., Hernandez, L.M., Tufenkji, N., 2018. Microplastics and nanoplastics in aquatic environments: aggregation, deposition, and enhanced contaminant transport. Environ. Sci. Technol. 52, 1704–1724.

Alimi, O.S., Farner, J.M., Tufenkji, N., 2021. Exposure of nanoplastics to freeze-thaw leads to aggregation and reduced transport in model groundwater environments. Water Res. 189, 116533.

Bläsing, M., Amelung, W., 2018. Plastics in soil: analytical methods and possible sources. Sci. Total Environ. 612, 422–435.

Bradford, S.A., Kim, H., Shen, C., Sasidharan, S., Shang, J., 2017. Contributions of nanoscale roughness to anomalous colloid retention and stability behavior. Langmuir 33, 10094–10105.

Bradford, S.A., Simunek, J., Bettahar, M., van Genuchten, M.T., Yates, S.R., 2003. Modeling colloid attachment, straining, and exclusion in saturated porous media. Environ. Sci. Technol. 37, 2242–2250.

Cai, L., He, L., Peng, S., Li, M., Tong, M., 2019. Influence of titanium dioxide nanoparticles on the transport and deposition of microplastics in quartz sand. Environ. Pollut. 253, 351–357.

Chen, C., Dynes, J.J., Wang, J., Sparks, D.L., 2014. Properties of Fe-organic matter associations via coprecipitation versus adsorption. Environ. Sci. Technol. 48, 13751–13759.
Chen, Y.L., Ma, J., Li, Y.T., Weng, L.P., 2019. Enhanced cadmium immobilization in saturated media by gradual stabilization of goethite in the presence of humic acid with increasing pH. Sci. Total Environ. 648, 358–366.
Cortes-Arriagada, D., 2021. Elucidating the co-transport of bisphenol A with polyethylene terephthalate (PET) nanoplastics: a theoretical study of the adsorption mechanism. Environ. Pollut. 270, 116192.
Davranche, M., Veclin, C., Pierson-Wickmann, A.C., El Hadri, H., Grassl, B., Rowenczyk, L., Dia, A., Ter Halle, A., Blancho, F., Reynaud, S., Gigault, J., 2019. Are nanoplastics able to bind significant amount of metals? The lead example. Environ. Pollut. 249, 940–948.
Dawson, A.L., Kawaguchi, S., King, C.K., Townsend, K.A., King, R., Huston, W.M., Nash, S.M.B., 2018. Turning microplastics into nanoplastics through digestive fragmentation by Antarctic krill. Nat. Commun. 9.
Della Torre, C., Bergami, E., Salvati, A., Faleri, C., Cirino, P., Dawson, K.A., Corsi, I., 2014. Accumulation and embryotoxicity of polystyrene nanoparticles at early stage of development of sea urchin embryos Paracentrotus lividus. Environ. Sci. Technol. 48, 12302–12311.
Derjaguin, B., Landau, L., 1941. Theory of the stability of strongly charged lyophobic sols and of the adhesion of strongly charged particles in solutions of electrolytes. Acta Physicochim. URSS.
Dong, Z., Qiu, Y., Zhang, W., Yang, Z., Wei, L., 2018. Size-dependent transport and retention of micron-sized plastic spheres in natural sand saturated with seawater. Water Res. 143, 518–526.
Dong, Z., Zhu, L., Zhang, W., Huang, R., Lv, X., Jing, X., Yang, Z., Wang, J., Qiu, Y., 2019. Role of surface functionalities of nanoplastics on their transport in seawater-saturated sea sand. Environ. Pollut. 255, 113177.
Duis, K., Coors, A., 2016. Microplastics in the aquatic and terrestrial environment: sources (with a specific focus on personal care products), fate and effects. Environ. Sci. Eur. 28, 2.
Foppen, J.W.A., Okletey, S., Schijven, J.F., 2006. Effect of goethite coating and humic acid on the transport of bacteriophage PRD1 in columns of saturated sand. J. Contam. Hydrol. 85, 287–301.
Frisch, M.J., Trucks, G.W., Schlegel, H.B., Scuseria, G.E., Robb, M.A., Cheeseman, J.R., Scalmani, G., Barone, V., Petersson, G.A., Nakatsuji, H., Li, X., Caricato, M., Marenich, A.V., Bloino, J., Janesko, B.G., Gomperts, R., Mennucci, B., Hratchian, H. P., Ortiz, J.V., Izmaylov, A.F., Sonnenberg, J.L., Williams-Young, D., Ding, F., Lipparini, F., Egidi, F., Goings, J., Peng, B., Petrone, A., Henderson, T., Ranasinghe, D., Zakrzewski, V.G., Gao, J., Rega, N., Zheng, G., Liang, W., Hada, M., Ehara, M., Toyota, K., Fukuda, R., Hasegawa, J., Ishida, M., Nakajima, T., Honda, Y., Kitao, O., Nakai, H., Vreven, T., Throssell Jr., K., Montgomery, J.A., Peralta, J.E., Ogliaro, F., Bearpark, M.J., Heyd, J.J., Brothers, E.N., Kudin, K.N., Staroverov, V.N., A, K.T., Kobayashi, R., Normand, J., Raghavachari, K., Rendell, A.P., Burant, J.C., Iyengar, S.S., Tomasi, J., Cossi, M., Millam, J.M., Klene, M., Adamo, C., Cammi, R., Ochterski, J.W., Martin, R.L., Morokuma, K., Farkas, O., Foresman, J.B., Fox, D.J., 2016. Gaussian, Inc., Wallingford CT.
Gao, M., Liu, Y., Dong, Y., Song, Z., 2021a. Effect of polyethylene particles on dibutyl phthalate toxicity in lettuce (Lactuca sativa L.). J. Hazard Mater. 401, 123422.
Gao, M., Xu, Y., Liu, Y., Wang, S., Wang, C., Dong, Y., Song, Z., 2021b. Effect of polystyrene on di-butyl phthalate (DBP) bioavailability and DBP-induced phytotoxicity in lettuce. Environ. Pollut. 268, 115870.
Gigault, J., Halle, A.T., Baudrimont, M., Pascal, P.Y., Gauffre, F., Phi, T.L., El Hadri, H., Grassl, B., Reynaud, S., 2018. Current opinion: what is a nanoplastic? Environ. Pollut. 235, 1030–1034.
Han, P., Wang, X., Cai, L., Tong, M., Kim, H., 2014. Transport and retention behaviors of titanium dioxide nanoparticles in iron oxide-coated quartz sand: effects of pH, ionic strength, and humic acid. Colloid. Surface. Physicochem. Eng. Aspect. 454, 119–127.
He, L., Rong, H., Wu, D., Li, M., Wang, C., Tong, M., 2020. Influence of biofilm on the transport and deposition behaviors of nano- and micro-plastic particles in quartz sand. Water Res. 178, 115808.
He, L., Wu, D., Rong, H., Li, M., Tong, M., Kim, H., 2018. Influence of nano- and microplastic particles on the transport and deposition behaviors of bacteria in quartz sand. Environ. Sci. Technol. 52, 11555–11563.
Hohenblum, P., Liebmann, B., Liedermann, M., 2015. Austrian Federal Ministry of Agriculture, Forestry, Environment and Water Management, Plastic and Microplastic in the Environment (Vienna).
Horton, A.A., Walton, A., Spurgeon, D.J., Lahive, E., Svendsen, C., 2017. Microplastics in freshwater and terrestrial environments: evaluating the current understanding to identify the knowledge gaps and future research priorities. Sci. Total Environ. 586, 127–141.
Hu, E., Shang, S., Fu, Z., Zhao, X., Nan, X., Du, Y., Chen, X., 2020. Cotransport of naphthalene with polystyrene nanoplastics (PSNP) in saturated porous media: effects of PSNP/naphthalene ratio and ionic strength. Chemosphere 245, 125602.
Huerta Lwanga, E., Gertsen, H., Gooren, H., Peters, P., Salanki, T., van der Ploeg, M., Besseling, E., Koelmans, A.A., Geissen, V., 2017a. Incorporation of microplastics from litter into burrows of Lumbricus terrestris. Environ. Pollut. 220, 523–531.
Huerta Lwanga, E., Gertsen, H., Gooren, H., Peters, P., Salánki, T., van der Ploeg, M., Besseling, E., Koelmans, A.A., Geissen, V., 2016. Microplastics in the terrestrial ecosystem: implications for Lumbricus terrestris (Oligochaeta, lumbricidae). Environ. Sci. Technol. 50, 2685–2691.
Huerta Lwanga, E., Mendoza Vega, J., Ku Quej, V., Chi, J.d.l.A., Sanchez del Cid, L., Chi, C., Escalona Segura, G., Gertsen, H., Salánki, T., van der Ploeg, M., Koelmans, A. A., Geissen, V., 2017b. Field evidence for transfer of plastic debris along a terrestrial food chain. Sci. Rep. 7, 14071.
Hüffer, T., Praetorius, A., Wagner, S., von der Kammer, F., Hofmann, T., 2017. Microplastic exposure assessment in aquatic environments: learning from similarities and differences to engineered nanoparticles. Environ. Sci. Technol. 51, 2499–2507.
Humphrey, W., Dalke, A., Schulten, K., 1996. VMD: Visual molecular dynamics. J. Mol. Graph. 14, 33–38.
Hurley, R.R., Nizzetto, L., 2018. Fate and occurrence of micro(nano)plastics in soils: knowledge gaps and possible risks. Curr. Opin. Environ. Sci. Health 1, 6–11.
Kamrani, S., Rezaei, M., Kord, M., Baalousha, M., 2018. Transport and retention of carbon dots (CDs) in saturated and unsaturated porous media: role of ionic strength, pH, and collector grain size. Water Res. 133, 338–347.
Lambert, S., Wagner, M., 2016. Characterisation of nanoplastics during the degradation of polystyrene. Chemosphere 145, 265–268.
Li, M., He, L., Zhang, M., Liu, X., Tong, M., Kim, H., 2019. Cotransport and deposition of iron oxides with different-sized plastic particles in saturated quartz sand. Environ. Sci. Technol. 53, 3547–3557.
Li, Q., Zeng, A., Jiang, X., Gu, X., 2021. Are microplastics correlated to phthalates in facility agriculture soil? Sci. Total Environ. 412, 125164.
Li, X., He, E., Xia, B., Van Gestel, C.A.M., Peijnenburg, W.J.G.M., Cao, X., Qiu, H., 2020a. Impact of CeO2 nanoparticles on the aggregation kinetics and stability of polystyrene nanoplastics: importance of surface functionalization and solution chemistry. Water Res. 186, 116324.
Li, X., He, E., Zhang, M., Peijnenburg, W.J.G.M., Liu, Y., Song, L., Cao, X., Zhao, L., Qiu, H., 2020b. Interactions of CeO2 nanoparticles with natural colloids and electrolytes impact their aggregation kinetics and colloidal stability. J. Hazard Mater. 386, 121973.
Li, X., Scheibe, T.D., Johnson, W.P., 2004. Apparent decreases in colloid deposition rate coefficients with distance of transport under unfavorable deposition Conditions: A general phenomenon. Environ. Sci. Technol. 38, 5616–5625.
Lu, T., Chen, F., 2012. Multiwfn: a multifunctional wavefunction analyzer. J. Comput. Chem. 33, 580–592.
Ma, J., Guo, H., Lei, M., Li, Y., Weng, L., Chen, Y., Ma, Y., Deng, Y., Feng, X., Xiu, W., 2018. Enhanced transport of ferrihydrite colloid by chain-shaped humic acid colloid in saturated porous media. Sci. Total Environ. 621, 1581–1590.
Ma, J., Guo, H., Lei, M., Wan, X., Zhang, H., Feng, X., Wei, R., Tian, L., Han, X., 2016. Blocking effect of colloids on arsenate adsorption during co-transport through saturated sand columns. Environ. Pollut. 213, 638–647.
Ma, J., Jing, Y., Gao, L., Chen, J., Wang, Z., Weng, L., Li, H., Chen, Y., Li, Y., 2020. Hetero-aggregation of goethite and ferrihydrite nanoparticles controlled by goethite nanoparticles with elongated morphology. Sci. Total Environ. 748, 141536.
Mayer, I., 1983. Charge, bond order and valence in the AB initio SCF theory. Chem. Phys. Lett. 97, 270–274.
Mayer, I., 1984. Bond order and valence: relations to Mulliken's population analysis. Int. J. Quant. Chem. 26, 151–154.
NIER, 2006. Environmental Monitoring of Endocrine Disrupting Chemicals.
Nowack, B., Bucheli, T.D., 2007. Occurrence, behavior and effects of nanoparticles in the environment. Environ. Pollut. 150, 5–22.
Oriekhova, O., Stoll, S., 2018. Heteroaggregation of nanoplastic particles in the presence of inorganic colloids and natural organic matter. Environ Sci-Nano 5, 792–799.
Oriekhova, O., Stoll, S., 2019. Heteroaggregation of CeO2 nanoparticles in presence of alginate and iron (III) oxide. Sci. Total Environ. 648, 1171–1178.
Peng, S., Wu, D., Ge, Z., Tong, M., Kim, H., 2017. Influence of graphene oxide on the transport and deposition behaviors of colloids in saturated porous media. Environ. Pollut. 225, 141–149.
Poater, A., Saliner, A.G., Cavallo, L., Poch, M., Sola, M., Worth, A.P., 2012. Tuning the electronic properties by width and length modifications of narrow- diameter carbon nanotubes for nanomedicine. Curr. Med. Chem. 19, 5219–5225.
Qian, X., Ma, J., Weng, L., Chen, Y., Ren, Z., Li, Y., 2020. Influence of agricultural organic inputs and their aging on the transport of ferrihydrite nanoparticles: from enhancement to inhibition. Sci. Total Environ. 719, 137440.
Rahman, M., Brazel, C.S., 2004. The plasticizer market: an assessment of traditional plasticizers and research trends to meet new challenges. Prog. Polym. Sci. 29, 1223–1248.
Rillig, M.C., 2012. Microplastic in terrestrial ecosystems and the soil? Environ. Sci. Technol. 46, 6453–6454.
Safiur Rahman, M., Whalen, M., Gagnon, G.A., 2013. Adsorption of dissolved organic matter (DOM) onto the synthetic iron pipe corrosion scales (goethite and magnetite): effect of pH. Chem. Eng. J. 234, 149–157.
Scheurer, M., Bigalke, M., 2018. Microplastics in Swiss slood plain soils. Environ. Sci. Technol. 52, 3591–3598.
Schwertmann, U., Cornell, R.M., 2008. Iron Oxides in the Laboratory: Preparation and Characterization. John Wiley & Sons.
Shani, C., Weisbrod, N., Yakirevich, A., 2008. Colloid transport through saturated sand columns: influence of physical and chemical surface properties on deposition. Colloid. Surface. 316, 142–150.
Shaniv, D., Dror, I., Berkowitz, B., 2021. Effects of particle size and surface chemistry on plastic nanoparticle transport in saturated natural porous media. Chemosphere 262, 127854.
Sharma, S., Chatterjee, S., 2017. Microplastic pollution, a threat to marine ecosystem and human health: a short review. Environ. Sci. Pollut. Control Ser. 24, 21530–21547.
Shellenberger, K., Logan, B.E., 2002. Effect of molecular scale roughness of glass beads on colloidal and bacterial deposition. Environ. Sci. Technol. 36, 184–189.
Shen, C., Li, B., Wang, C., Huang, Y., Jin, Y., 2011. Surface roughness effect on deposition of nano- and micro-sized colloids in saturated columns at different solution ionic strengths. Vadose Zone J. 10, 1071–1081.

Song, L., Johnson, P.R., Elimelech, M., 1994. Kinetics of colloid deposition onto heterogeneously charged surfaces in porous media. Environ. Sci. Technol. 28, 1164–1171.
Song, Z., Yang, X., Chen, F., Zhao, F., Zhao, Y., Ruan, L., Wang, Y., Yang, Y., 2019. Fate and transport of nanoplastics in complex natural aquifer media: effect of particle size and surface functionalization. Sci. Total Environ. 669, 120–128.
Steinmetz, Z., Wollmann, C., Schaefer, M., Buchmann, C., David, J., Troger, J., Munoz, K., Fror, O., Schaumann, G.E., 2016. Plastic mulching in agriculture. Trading short-term agronomic benefits for long-term soil degradation? Sci. Total Environ. 550, 690–705.
Tan, Z., Yin, Y., Guo, X., Wang, B., Shang, H., Xu, J., Zhao, Q., Liu, J., Xing, B., 2019. Natural organic matter inhibits aggregation of few-layered black phosphorus in mono- and divalent electrolyte solutions. Environ. Sci.: Nano 6, 599–609.
Tong, M., He, L., Rong, H., Li, M., Kim, H., 2020a. Transport behaviors of plastic particles in saturated quartz sand without and with biochar/Fe3O4-biochar amendment. Water Res. 169, 115284.
Tong, M., Li, T., Li, M., He, L., Ma, Z., 2020b. Cotransport and deposition of biochar with different sized-plastic particles in saturated porous media. Sci. Total Environ. 713, 136387.
Tufenkji, N., Elimelech, M., 2004. Deviation from the classical colloid filtration theory in the presence of repulsive DLVO interactions. Langmuir 20, 10818–10828.
Verwey, E.J.M., Overbeek, J.T.G., 1948. Theory of the Stability of Lyophobic Colloids. Elsevier, Amsterdam, The Netherlands.
Wang, D., Bradford, S.A., Harvey, R.W., Gao, B., Cang, L., Zhou, D., 2012. Humic acid facilitates the transport of ARS-labeled hydroxyapatite nanoparticles in iron oxyhydroxide-coated sand. Environ. Sci. Technol. 46, 2738–2745.
Wang, L., Li, Y., Weng, L., Sun, Y., Ma, J., Chen, Y., 2019. Using chromatographic and spectroscopic parameters to characterize preference and kinetics in the adsorption of humic and fulvic acid to goethite. Sci. Total Environ. 666, 766–777.
Witthayaphirom, C., Chiemchaisri, C., Chiemchaisri, W., Ogata, Y., Ebie, Y., Ishigaki, T., 2020. Long-term removals of organic micro-pollutants in reactive media of horizontal subsurface flow constructed wetland treating landfill leachate. Bioresour. Technol. 312, 123611.
Wright, S.L., Thompson, R.C., Galloway, T.S., 2013. The physical impacts of microplastics on marine organisms: a review. Environ. Pollut. 178, 483–492.
Wu, X., Lyu, X., Li, Z., Gao, B., Zeng, X., Wu, J., Sun, Y., 2020. Transport of polystyrene nanoplastics in natural soils: effect of soil properties, ionic strength and cation type. Sci. Total Environ. 707, 136065.
Zeng, F., Cui, K.Y., Xie, Z.Y., Wu, L.N., Luo, D.L., Chen, L.X., Lin, Y.J., Liu, M., Sun, G.X., 2009. Distribution of phthalate esters in urban soils of subtropical city, Guangzhou, China. J. Hazard Mater. 164, 1171–1178.
Zhang, F., Wang, Z., Wang, S., Fang, H., Wang, D., 2019. Aquatic behavior and toxicity of polystyrene nanoplastic particles with different functional groups: complex roles of pH, dissolved organic carbon and divalent cations. Chemosphere 228, 195–203.
Zhou, B., Zhao, L., Wang, Y., Sun, Y., Li, X., Xu, H., Weng, L., Pan, Z., Yang, S., Chang, X., Li, Y., 2020. Spatial distribution of phthalate esters and the associated response of enzyme activities and microbial community composition in typical plastic-shed vegetable soils in China. Ecotoxicol. Environ. Saf. 195, 110495.
Zorníková, G., Jarošová, A., Hřivna, L., 2014. Distribution of phthalic acid esters in agricultural plants and soil. Acta Univ. Agric. Silvic. Mendelianae Brunensis 59, 233–238.